PNAS
www.pnas.org

Supplementary Information for

Weber-Fechner gain control enhances the fidelity of combinatorial odor coding

Nirag Kadakia and Thierry Emonet

Nirag Kadakia.
E-mail: nirag.kadakia@yale.edu

This PDF file includes:

Supporting Information Text

Mathematical model

Model of odor binding, Or/Orco activation, and ORN firing. We model an odor as an N-dimensional vector $\mathbf{s} = [s_1, ..., s_N]$, where $s_i > 0$ are the concentrations of individual volatile molecules (odorants) comprising the odor. The olfactory sensory system is modeled as a collection of M distinct Or/Orco complexes indexed by the sub index $a = 1, ..., M$, each of which can be bound with any one of the odorant molecules, and can be either active (firing) or inactive (quiescent). At first we assume there is one binding site per complex; this will be generalized to many sites. We consider the binding and activation processes to be in equilibrium, assigning each state a corresponding Boltzmann weight, where the zero of energy is set by the unbound, inactive state C_a. These weights are:

$$\begin{aligned} &C_a && 1 \\ &C_a^* && \exp(-\beta\epsilon_a) \\ &C_a s_i && \exp(-\beta(-E_{ai} - \mu_i)) \\ &C_a^* s_i && \exp(-\beta(-(E_{ai}^* - \epsilon_a) - \mu_i), \end{aligned} \quad [1]$$

where ϵ_a (assumed positive) is the free energy difference between the active and inactive conformation of the unbound receptor, and E_{ai} and E_{ai}^* are the free energy differences (assumed positive) between the unbound and bound state for the inactive and active receptor, respectively. $\mu_i = \mu_0 + \beta^{-1}\log(s_i/s_0)$ is the chemical potential for odorant species i in terms of a reference chemical potential μ_0 at concentration s_0, $s_0 \exp(-\beta\mu_0) = s_i \exp(-\beta\mu_i)$, which can be traded for the thermodynamic-relevant disassociation constants $K_{ai} = s_0 e^{\beta(-E_{ai} - \mu_0)}$. Adding up contributions from all i odorants, the active fraction is:

$$A_a = \frac{C_a^* + \sum_i C_a^* s_i}{C_a + \sum_i C_a s_i + C_a^* + \sum_i C_a^* s_i} = \left(1 + e^{\epsilon_a} \frac{1 + \sum_i^N \frac{s_i}{K_{ai}}}{1 + \sum_i^N \frac{s_i}{K_{ai}^*}}\right)^{-1}, \quad [2]$$

where we have expressed free energies in units of $k_B T = \beta^{-1}$ for notational convenience.

This expression can be generalized for the case of multiple, independent binding sites through some simple combinatorial factors. Consider first an odorant i which can bind one of two locations on receptor a. There are then 4 possible inactive states: both sites unbound, site 1 bound, site 2 bound, both sites bound. Combined with the active states, there are therefore 8 states for odorant i and receptor a, with energies:

$$\begin{aligned} &\text{active} && \{1, \quad -E_{ai} - \mu_i, \quad -E_{ai} - \mu_i, \quad -2E_{ai} - 2\mu_i\} \\ &\text{inactive} && \{\epsilon_a, \quad -(E_{ai}^* - \epsilon_a) - \mu_i, \quad -(E_{ai}^* - \epsilon_a) - \mu_i, \quad -(2E_{ai}^* - \epsilon_a) - 2\mu_i\} \end{aligned} \quad [3]$$

In the active fraction, Eq. 2, the Boltzmann factors combine through the binomial theorem, giving (for a single odorant environment i):

$$A_a(\text{odorant } i, \text{ 2 binding sites}) = \left(1 + e^{\epsilon_a} \frac{(1 + \frac{s_i}{K_{ai}})^2}{(1 + \frac{s_i}{K_{ai}^*})^2}\right)^{-1}. \quad [4]$$

This expression generalizes for an arbitrary number of odorants and independent binding sites through the appropriate combinatorial factors, giving an active fraction of

$$A_a(N \text{ odorants}, R \text{ binding sites}) = \left[1 + e^{\epsilon_a} \left(\frac{1 + \sum_i^N \frac{s_i}{K_{ai}}}{1 + \sum_i^N \frac{s_i}{K_{ai}^*}}\right)^R\right]^{-1}. \quad [5]$$

Finally, firing rate dynamics are assumed linear-nonlinear:

$$r_a(t) = f\left(\int^t h(t - \tau) A(\tau) d\tau\right), \quad [6]$$

where $h(t)$ and f are a temporal filter and rectifying linear unit (with threshold $\theta = 5$ Hz) as noted in the main text.

Compressed sensing decoding

Compressed sensing decoding of ORN response. Compressed sensing (CS) addresses the problem of determining a sparse signal from a set of linear measurements, when the number of measurements is less than the signal dimension. Specifically, it is a solution to

$$\mathbf{y} = \mathbf{R}\mathbf{x}, \quad [7]$$

where $\mathbf{x} \in \mathbb{R}^N$ and $\mathbf{y} \in \mathbb{R}^M$ are vectors of signals and responses, respectively, and $\mathbf{R}$ is the measurement matrix. Since measurements are fewer than signal components, then $M < N$, whereby $\mathbf{R}$ is wide rectangular and so Eq. 7 cannot be simply

inverted to produce $\mathbf{x}$. The idea of CS is to utilize the knowledge that $\mathbf{x}$ is sparse, i.e.g only K of its components, $K \ll N$ are nonzero. Both the measurements and sparsity are thus combined into a single constrained optimization routine:

$$\hat{x}_i = \text{argmin} \sum_i^N |x_i| \quad \text{such that } \mathbf{y} = \mathbf{R}\mathbf{s} \tag{8}$$

where $\hat{x}_i$ are the optimal estimates of the signal components and the sum, which is known as the L_1 norm of $\mathbf{x}$, is a natural metric of sparsity (1).

The L_1 norm is a convex operation and the constraints are linear, so the optimization has a unique global minimum. To incorporate the nonlinear response of our encoding model into this linear framework, we assume that the responses are generated through the full nonlinear steady state response, Eq. 2- 6, but that the measurement matrix $\mathbf{R}$ needed for decoding uses a linear approximation of this transformation. Expanding Eq. 6 around $\mathbf{s}_0 = \mathbf{s} - \Delta\mathbf{s}$ gives

$$\Delta r_a(t) = r_a(\mathbf{s}(t)) - r_a(\mathbf{s}_0(t)) \tag{9}$$

$$\Delta r_a(t) = \int^t d\tau h(t-\tau) \sum_i^N \frac{dA_{ai}}{ds}\Big|_{\mathbf{s}_0} \Delta s_i \tag{10}$$

$$r_a(\mathbf{s}_0) = \int^t d\tau h(t-\tau) \sum_i^N A_{a0} \tag{11}$$

$$\frac{dA_{ai}}{ds}\Big|_{\mathbf{s}_0} = A_{a0}(1-A_{a0}) \left[\frac{1}{K_{ai}} \left(1 + \sum_j \frac{s_{0,j}}{K_{aj}} \right)^{-1} - \frac{1}{K^*_{ai}} \left(1 + \sum_j \frac{s_{0,j}}{K^*_{aj}} \right)^{-1} \right] \tag{12}$$

where $A_{a0} = A(\mathbf{s}_0)$ and where Eqs. 10 and 11 hold only for integrands above 5 Hz (and are zero below), as per the linear rectifier f. We assume that the neural decoder has access to background $\mathbf{s}_0$, presumed learned (this assumption can be relaxed; see below), and to the linearized response matrix, Eq. 12, but must infer the excess signals Δs_i from excess ORN firing rates $\Delta r_a(t)$. Thus, this corresponds to the CS framework (Eq. 8) via $\Delta\mathbf{r} \to \mathbf{y}$, $\Delta\mathbf{s} \to \mathbf{x}$, and $A'_{ai}\big|_{\mathbf{s}_0} \to \mathbf{R}$. We optimize the cost function in Eq. 8 using sequential least squares programming, implemented in Python through using the scientific package SciPy.

Iterative Hard Tresholding (IHT) and the Restricted Isometry Property in compressed sensing. We stress that the purpose of response linearization is simply to apply compressed sensing reconstruction directly using linear programming, without worrying about issues of local minima in Eq. 8. This allows us to isolate the impact of Weber Law adaptation from the particularities of the numerics. An alternate technique for compressed signal reconstruction, *iterative hard thresholding* (IHT), does not minimize the constrained L_1 norm directly, rather applying a hard threshold to an iteratively updated signal estimate (2). IHT can be generalized straightforwardly to nonlinear constraints, and would actually dispense with the need for a learned background $\mathbf{s}_0$, simply initializing the iterations from $\mathbf{s}_0 = \mathbf{0}$. Remarkably, this technique works quite well even for non-linear measurements (3). We demonstrate the applicability of the IHT algorithm to our odor decoding system in Fig. S8, which reproduces qualitatively the findings in the main text. For these calculations, no background odor was assumed, each iterative decoding being initialized at the zero vector.

IHT provides an alternate computational technique of nonlinear CS, which could be used to both extend and verify our results. Further, it allows us to illustrate why Weber Law adaptation maintains signal reconstruction fidelity in our olfactory sensing model. Like CS using L_1-norm minimization, IHT exhibits amenable reconstruction and convergence properties under the guarantee of the so-called restricted isometry property (RIP) (4). Loosely, RIP measures the closeness of matrix operator to an orthogonal transformation when acting on sparse vectors. The degree to which RIP is satisfied can be understood in terms of the spectrum of a measurement matrix $\mathbf{A}$. In particular, if λ_i are the eigenvalues of $\mathbf{A}_k^T\mathbf{A}_k$, where $\mathbf{A}_k$ is any $k \times m$ submatrix of $\mathbf{A}$, and

$$1 - \delta_k \leq \lambda_{min} \leq \lambda_{max} \leq 1 + \delta_k$$

is satisfied for some δ_k, then $\mathbf{A}$ satisfies the RIP with constant δ_k. Plainly, the RIP states that the eigenvalues of $\mathbf{A}_k^T\mathbf{A}_k$, when acting on k-sparse vectors, are centered around 1. Thus, to intuit why signal reconstruction breaks down in the non-adaptive sensing system, we can investigate the eigendecomposition of various linearizations of the measurement matrix. We do this now, starting with a brief description of the IHT.

In the linear setting, IHT seeks sparse signals via the following iterative procedure (2):

$$\mathbf{x}_{k+1} = H_K(\mathbf{x}_k + \mu\mathbf{R}^T(\mathbf{x}_k + (\mathbf{y} - \mathbf{R}\mathbf{x}_k))) \tag{13}$$

where $\mathbf{x}_k$ is the kth estimate of the sparse signal $\mathbf{x}$, μ is a step size for the iterations, and $\mathbf{y}$, $\mathbf{R}$ are as defined above. $H_k(\cdot)$ is a thresholding function which sets all but the largest K values of its argument to zero. The nonlinear extension to IHT is (3):

$$\mathbf{x}_{k+1} = H_K(\mathbf{x}_k + \mu\mathbf{A}_{\mathbf{x}_n}^T(\mathbf{x}_k + (\mathbf{y} - A(\mathbf{x}_k)))), \tag{14}$$

where A is a nonlinear sensing function and $\mathbf{A}_{\mathbf{x}_n}$ is a linearization of A about the point $\mathbf{x}_n$. Reconstructibility for k-sparse signals is guaranteed if $\mathbf{A}_{\mathbf{x}_n}$ satisfies RIP for all $\mathbf{x}_n$ and all k-sparse vectors (2). To get a sense of how this is preserved in the adaptive system, we calculate the eigenvalues for 1000 choices of $\mathbf{x}_n$, acting on random signals of given sparsity K (Fig. S7). Since the RIP is sensitive to constant scalings of the measurement matrix (while the actual estimation problem is not), we scaled all columns of $\mathbf{A}_{\mathbf{x}_n}$ to norm unity (5). This normalizes the eigenvalues of $\mathbf{A}_{\mathbf{x}_n}^T \mathbf{A}_{\mathbf{x}_n}$ to center near unity before calculating the eigendecomposition, allowing us to assess the degree to which the RIP is satisfied. This scaled matrix can be used directly in Eq. 14 (3, 5). The spectra of these matrices indicates that the RIP becomes far more weakly satisifed in the non-adaptive system than in the adaptive one, for sufficient odor complexity and intensity.

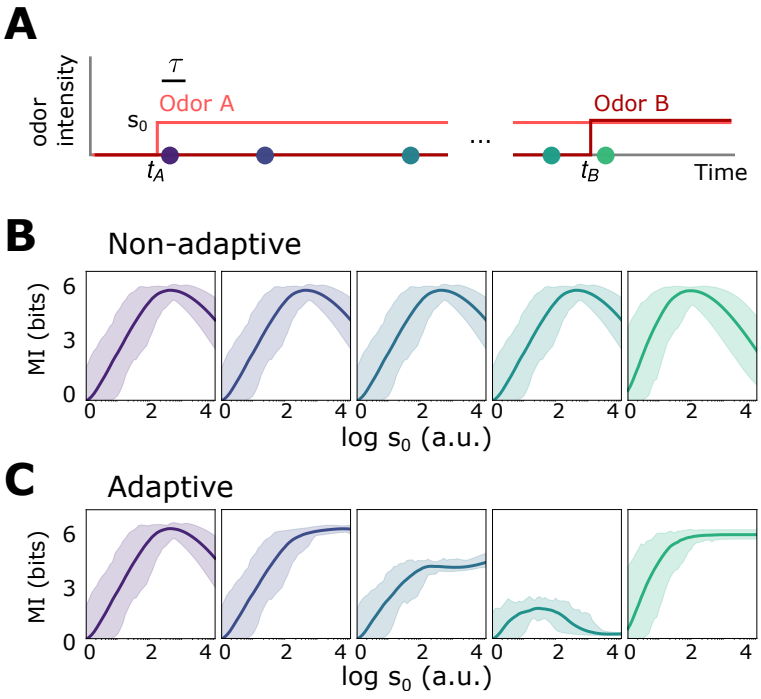

Fig. S1. Front-end adaptive feedback preserves information capacity of the ORN sensing repertoire. Mutual information between signal $\mathbf{s}(t) = \mathbf{s}_A(t) + \mathbf{s}_B(t)$ and response $\mathbf{r}(t)$ is calculated at various points in time t for an odor environment consisting of two step odors, A and B. **A** Odor A, with concentration $\mathbf{s}_A(t)$, turns on at time t_A and a odor B, with concentration $\mathbf{s}_B(t)$, turns on at some later time t_B. Both odors have similar intensities $\sim s_0$ and similar molecular complexity ($k = 4$). **B** Mutual information as a function of s_0 for the non-adaptive system, respectively, at different time points after t_A, corresponding to the dots in A. The mutual information carried by distinct ORNs is represented by the shaded region; their average is plotted by the heavy line. In the non-adaptive system, the mutual information peaks in the regime of high sensitivity after the arrival of odor A (purple, blue), and shifts leftward with the onset of odor B (teal, green). The leftward shifts occurs since stronger signals are more prone to response saturation (compromising information transfer) as odor B arrives. **C** Same as B, now for the adaptive system. The MI mimics the non-adaptive case at the onset of odor A, before adaptation has kicked in (purple). As the system adapts and responses decrease toward baseline, previously saturating signal intensities now cross the regime of maximal sensitivity, which therefore shifts rightward to higher s_0 (dark blue). Much later, but before the arrival of odor B, the ORNs that responded now fire at a similar adapted firing rate ~ 30 Hz, irrespective of odor identity, so the mutual information drops to zero. However, having now adjusted its sensitivity to the presence of odor A, the system can respond appropriately to odor B: the MI at t_B is nearly 6 bits across decades of concentration immediately following t_B (green).

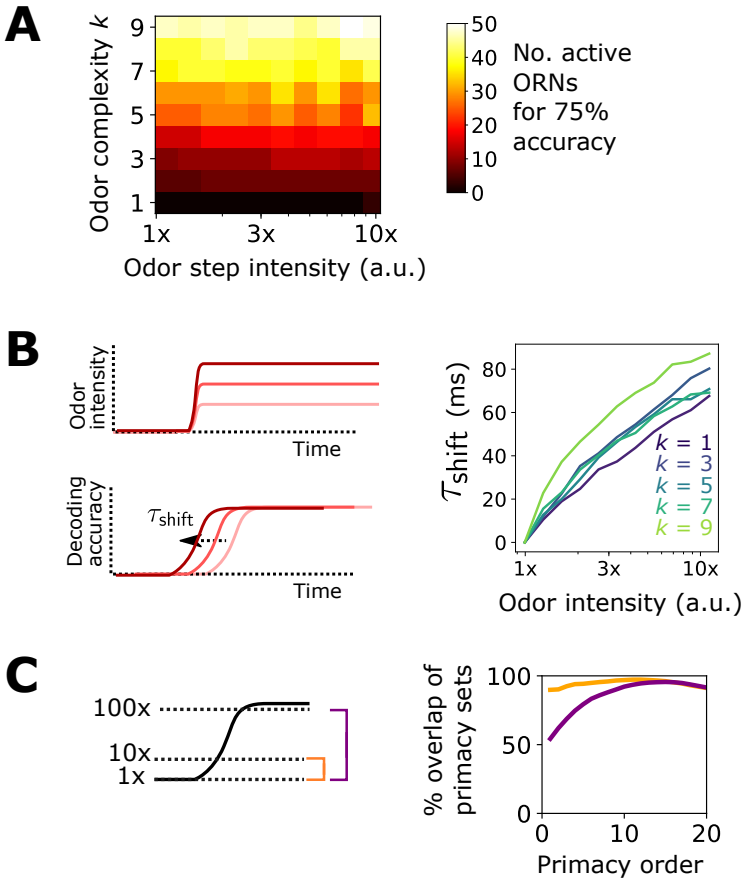

Fig. S2. Additional results pertaining to the primacy coding hypothesis. **A** Percent of active ORNs required for 75% accuracy of a steep sigmoidal odor step, as a function of odor step intensity and odor complexity. For low complexities, a primacy set of fewer ORNs may be sufficient to decode the full odor signal; for higher complexities, the entire ORN repertoire is required. **B** In the primacy coding hypothesis, the primacy set is realized sooner for stronger odor signals, so odors are decoded earlier in time, resulting in a perceptual time shift with increasing odor concentration (6). We also find this shift in our compressed sensing decoding framework (right plot), which rises monotonically with step height for various odor complexities, in agreement with primacy coding. **C** The consistency of a primacy code across changes in background odor concentration, in a system with Weber Law adaptation. We calculate the primacy set for odor A (step odor; black) in the presence of either a weak, medium, or strong background (dotted lines; 1x, 10x, 100x a.u.), assuming the system has adapted its response to the background as described in the main text. Averaged across odor A identities, primacy sets for odor A when in the 1x background are nearly identical to those when odor A is in the 10x background (right plot; yellow). The same holds true when comparing the 1x and 100x backgrounds, for sufficiently large primacy order, above 8 or so right plot; purple). This indicates that Weber Law adaptation preserves primacy codes across disparate environmental conditions.

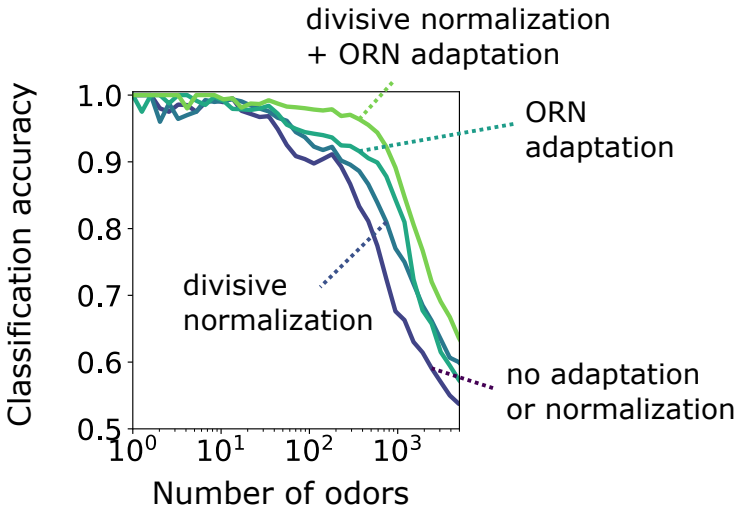

Fig. S3. Accuracy of binary classification by odor valence, for odors whose concentrations span a narrow range of concentrations (1 order of magnitude). Accuracy is plotted as a function of the number of distinct odor identities classified by the trained network, in systems with only ORN adaptation, only divisive normalization, both or neither. Decoding gains conferred by divisive normalization and/or ORN adaptation are much smaller than when odors span a much larger range of concentrations, as shown in the main text.

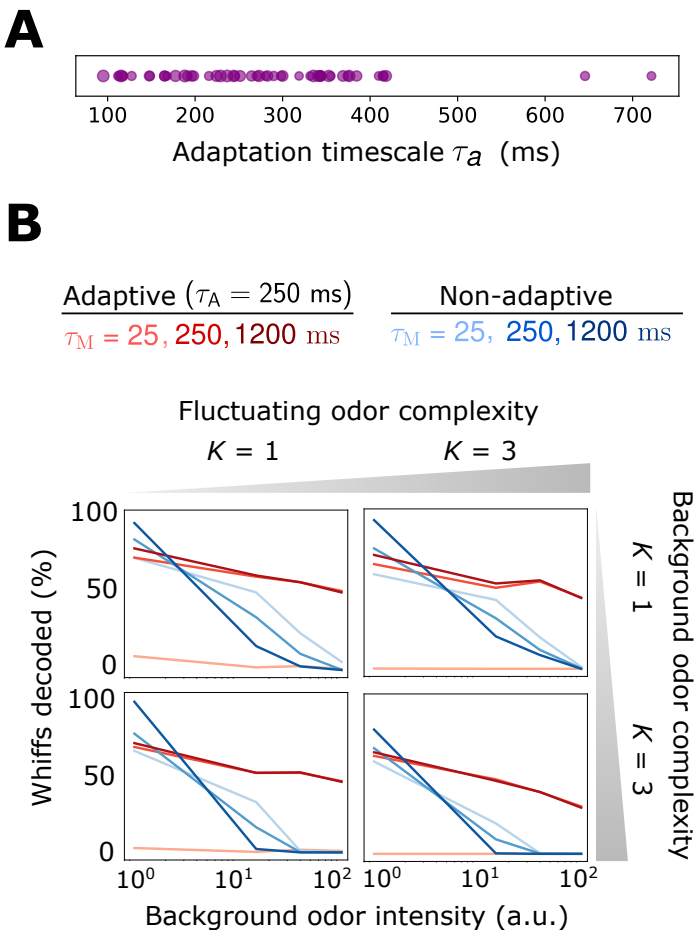

Fig. S4. Decoding accuracy for system with broader distribution of adaptive timescales τ. **A** Distribution of timescales for all ORNs a (purple dots). Here, $\tau_a \sim= 10^X$ where $\tau = 250$ ms as in the main text and $X \sim \mathcal{N}(0, 0.2)$. **B** Individual plots show the percent of accurately decoded odor whiffs (same fluctuating odor signal used in the main text) as a function of background odor intensity, for the non-adaptive (blue) and adaptive (red) systems, for different τ_M (line shades). Plots are arrayed by the complexity of the naturalistic signal (column-wise) and the complexity of the background odor (row-wise).

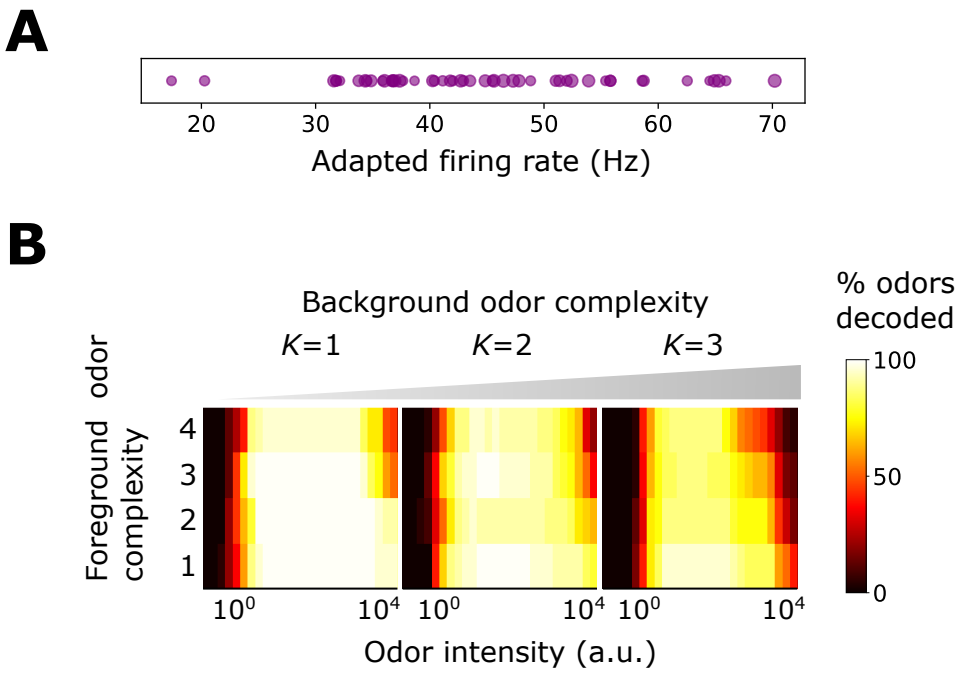

Fig. S5. Benefits conferred by Weber-Fechner adaptation remain for a broader distribution of baseline firing rates A_{a0}, now assumed to be ORN-dependent and chosen from a normal distribution. **A** Distribution of A_{a0}. **B** Decoding accuracy of foreground odors in the presence of background odors.

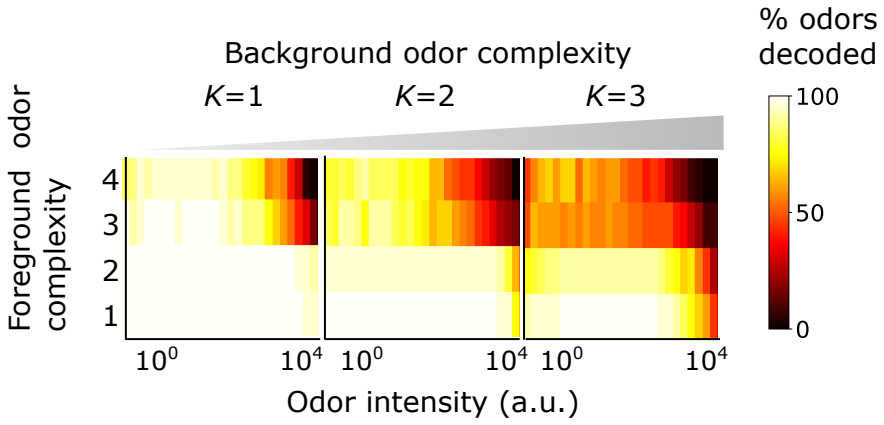

Fig. S6. Benefits conferred by Weber-Fechner adaptation remain for 2 binding sites per receptor. This might conceivably occur in insect olfactory receptors, heterotetramers consisting of 4 Orco/Or subunits that gate a central ion channel pathway (7). Plotted is the decoding accuracy of foreground odors in the presence of background odors.

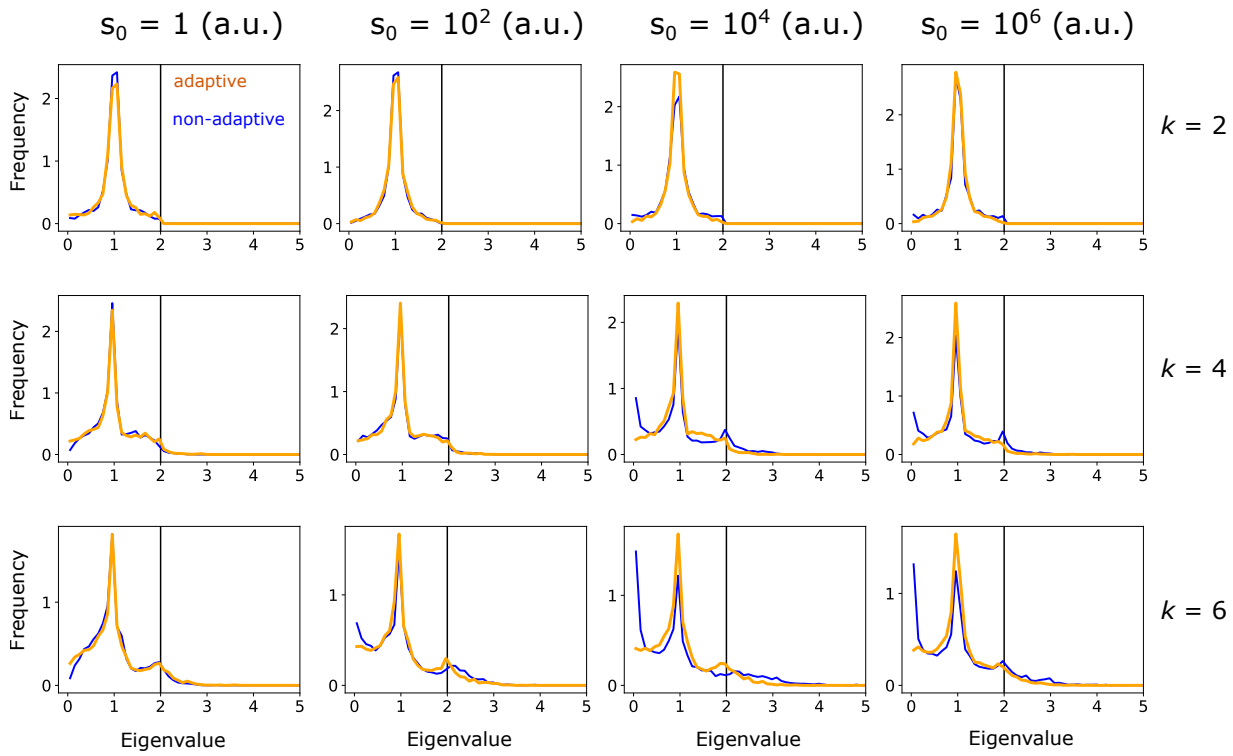

Fig. S7. Eigenvalue distribution of $\mathbf{A}_{\mathbf{x}_n}^T \mathbf{A}_{\mathbf{x}_n}$, where $\mathbf{A}_{\mathbf{x}_n}$ is a $m \times k$ submatrix of the column-normalized linearized ORN response matrix $\mathbf{A}$, evaluated at the linearization point $\mathbf{x}_n$. Note that $\mathbf{x}_n$ is k-sparse, but its components do not necessarily align with the k columns chosen for the sub-matrix. Eigenvalues are calculated for the adaptive (orange) and non-adaptive (blue) systems, for 1000 randomly chosen linearization points $\mathbf{x}_n$ and submatrices. Plots are arranged for various odor sparsities (by row) and odor intensities (by column). The restricted isometry property is satisfied when the eigenvalues lie between 0 and 2 (black vertical line), and is more strongly satisfied the more centered the distribution is around unity. The increase in near-zero eigenvalues for the non-adaptive system at higher odor complexities and intensities (lower right plots) indicates the weaker fulfillment of the restricted isometry property for thhse signals, and leads to higher probability of failure in compressed sensing signal reconstruction.

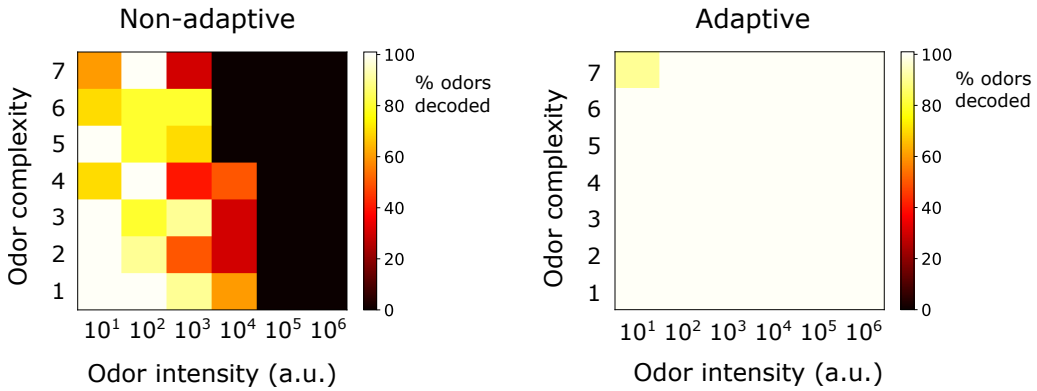

Fig. S8. Decoding of odor signals (no background odors) using the IHT algorithm (2, 3) qualitatively reproduces the results from the main text, which used traditional CS with background linearization. In the adaptive case, IHT actually exhibits superior accuracy to traditional CS, though IHT demands more compute time. The results here show odor decoding accuracy for sparse odor signals of given complexity and intensity, averaged over 10 distinct identities. Odors are considered accurately decoded if the K sparse components are estimated within 25% and the components not in the mixture are estimated below 10% of s_0. The iterative algorithm was initialized at $\hat{\mathbf{x}} = \mathbf{0}$ and run forward until $\hat{\mathbf{x}}$ was stationary, or 10000 iterations were reached. Step size μ in Eq. 14 was set to $s_0/20$. At each step, the linearized response ($\mathbf{A}_{\mathbf{x}_n}$ in Eq. 14) was evaluated at the result of the previous iteration. IHT also requires an assumption on the number of components in the mixture (which defines $H_K(\cdot)$ in Eq. 14); here, that was set to twice the actual sparsity of true signal.

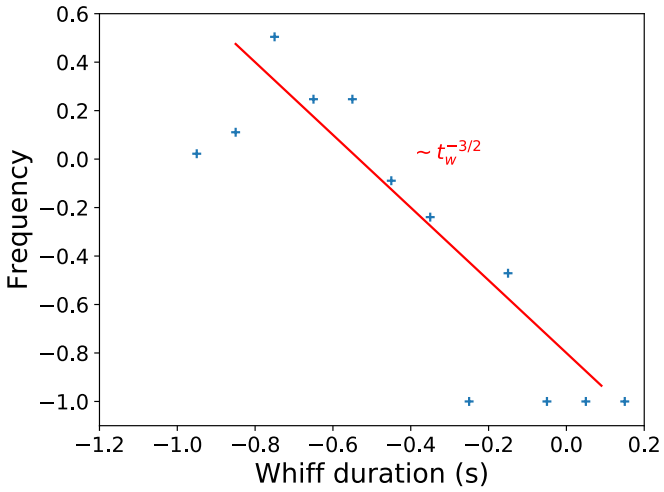

Fig. S9. Distribution of whiff durations in naturalistic stimulus, compared to the theoretical prediction (8).

References

1. Donoho D (2006) Compressed sensing. *IEEE Transactions on Information Theory* 52(4):1289–1306.
2. Blumensath T, Davies ME (2009) Iterative hard thresholding for compressed sensing. *Applied and Computational Harmonic Analysis* 27(3):265 – 274.
3. Blumensath T (2013) Compressed sensing with nonlinear observations and related nonlinear optimization problems. *IEEE Transactions on Information Theory* 69(6).
4. Candes E, Romberg J, Tao T (2006) Stable signal recovery from incomplete and inaccurate measurements. *Communications on Pure and Applied Mathematics* LIX:1207–1223.
5. Blumensath T, Davies ME (2009) How to use the iterative hard thresholding algorithm in *Proceedings of SPARS'09 - Signal Processing with Adaptive Sparse Structured Representations (Saint Malo, France, April 2009)*.
6. Wilson CD, Serrano GO, Koulakov AA, Rinberg D (2017) A primacy code for odor identity. *Nature Communications* 8(1):1477.
7. Butterwick JA, et al. (2018) Cryo-EM structure of the insect olfactory receptor Orco. *Nature* 560:447–452.
8. Celani A, Villermaux E, Vergassola M (2014) Odor landscapes in turbulent environments. *Phys. Rev. X* 4(4):041015.